Naval Research Laboratory

Washington, DC 20375-5000 NRL Memorandum Report 6188 DATE: 30 August 1988

(2)

DEVELOPMENTS IN HOT-FILM ANEMOMETRY MEASUREMENTS OF HYDROACOUSTIC PARTICLE MOTION

Pieter S. Dubbelday
Virgil V. Apostolico
and
Dean L. Diebel

Naval Research Laboratory
Underwater Sound Reference Detachment
P. O. Box 568337
Orlando, Florida 32856-8337

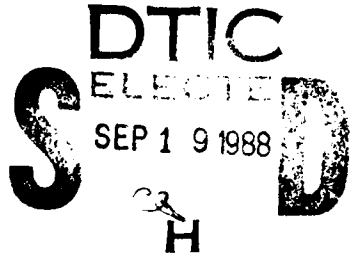

UNCLASSIFIED
SECURITY CLASSIFICATION OF THIS PAGE

REPORT DOCUMENTATION PAGE

Form Approved OMB No 0704-0188

1a. REPORT SECURITY CLASSIFICATION: UNCLASSIFIED	1b. RESTRICTIVE MARKINGS: N/A
2a. SECURITY CLASSIFICATION AUTHORITY: N/A	3. DISTRIBUTION / AVAILABILITY OF REPORT: Approved for public release; distribution unlimited.
2b. DECLASSIFICATION / DOWNGRADING SCHEDULE: N/A	
4. PERFORMING ORGANIZATION REPORT NUMBER(S): NRL MEMORANDUM REPORT NO. 6188	5. MONITORING ORGANIZATION REPORT NUMBER(S)
6a. NAME OF PERFORMING ORGANIZATION: NAVAL RESEARCH LABORATORY, Underwater Sound Reference Det / 6b. OFFICE SYMBOL (If applicable): Code 5993	7a. NAME OF MONITORING ORGANIZATION
6c. ADDRESS (City, State, and ZIP Code): P.O. Box 568337, Orlando, Florida 32856-8337	7b. ADDRESS (City, State, and ZIP Code)
8a. NAME OF FUNDING / SPONSORING ORGANIZATION: Office of Naval Technology / 8b. OFFICE SYMBOL (If applicable): ONT 230	9. PROCUREMENT INSTRUMENT IDENTIFICATION NUMBER
8c. ADDRESS (City, State, and ZIP Code): Arlington, VA 22217-5000	10. SOURCE OF FUNDING NUMBERS: PROGRAM ELEMENT NO: 62314N; PROJECT NO: ; TASK NO: RL3A/01; WORK UNIT ACCESSION NO: (59)-0593

11. TITLE (Include Security Classification)
DEVELOPMENTS IN HOT-FILM ANEMOMETRY MEASUREMENT OF HYDROACOUSTIC PARTICLE MOTION

12. PERSONAL AUTHOR(S)
P.S. Dubbelday, V.V. Apostolico, and D.L. Diebel

13a. TYPE OF REPORT	13b. TIME COVERED	14. DATE OF REPORT (Year, Month, Day)	15. PAGE COUNT
Final	FROM Jan 1986 TO Sep 1987	30 August 1988	24

16. SUPPLEMENTARY NOTATION

17. COSATI CODES			18. SUBJECT TERMS (Continue on reverse if necessary and identify by block number)
FIELD	GROUP	SUB-GROUP	Hot-film anemometry Hydroacoustic particle motion Acoustic transduction

19. ABSTRACT (Continue on reverse if necessary and identify by block number)

It has been shown [P.S. Dubbelday, J. Acoust. Soc. Am. **79**, 2060-2066 (1986)] that hot-film anemometry may be used to measure particle motion in hydroacoustic fields. Since the cylindrical sensors used thus far are very fragile, the method is little suited for use outside the laboratory. The measurement of the response of a more rugged conical sensor is reported here. Another way of protecting the sensor consists of packaging the sensor in a rubber liquid-filled boot. This also prevents fouling and bubble formation on the heated film. The response shows a resonance at low frequency, ascribed to the liquid-filled boot, which may be used for enhanced response in a limited frequency region. The response of a hot-film anemometer to vertical hydroacoustic particle motion is influenced by free convection, which acts as a bias flow. The output was shown to be proportional to particle displacement for a wide range of parameters. It was expected that an imposed bias flow would increase the output and remove the
(continued on reverse)

20. DISTRIBUTION / AVAILABILITY OF ABSTRACT: ☒ UNCLASSIFIED/UNLIMITED ☐ SAME AS RPT ☐ DTIC USERS	21. ABSTRACT SECURITY CLASSIFICATION: UNCLASSIFIED
22a. NAME OF RESPONSIBLE INDIVIDUAL: Dr. Pieter S. Dubbelday	22b. TELEPHONE (Include Area Code): (407)857-5197 / 22c. OFFICE SYMBOL: NRL-USRD Code 5993

DD Form 1473, JUN 86 *Previous editions are obsolete.* SECURITY CLASSIFICATION OF THIS PAGE
UNCLASSIFIED

ITEM 19 ABSTRACT continued
dependence on the direction of gravity. Therefore, a hot-film sensor (diameter d) was subjected to an underwater jet from a nozzle. The output showed a transition from being proportional to particle speed, to being proportional to particle displacement, depending on the angular frequency ω and imposed flow speed U. The transition takes place when a dimensionless number Ω, defined as $\Omega = \omega d/U$ is of order 1.

CONTENTS

DEVELOPMENTS IN HOT-FILM ANEMOMETRY MEASUREMENT OF HYDROACOUSTIC PARTICLE MOTION

INTRODUCTION

In previous publications [1,2] a description was presented of the application of hot-film anemometry (HFA) to the measurement of particle motion in hydroacoustic fields. The method of hot-film (or hot-wire) anemometry relies on the fact that cooling of an electrically heated film or wire depends on the motion of the surrounding medium (gas or liquid). Figure 1 shows the appearance of a cylindrical hot-film sensor with its support. This configuration was used thus far in the experiments. The quartz cover makes the sensor usable in conducting liquids like water. In most cases, the sensor is operated in a constant-temperature mode (Fig. 2). It forms one component of a bridge, where the control resistor R_1 determines the temperature difference between sensor and medium. A differential amplifier keeps the bridge balanced by supplying a voltage (V) to the bridge. This holds the sensor resistance constant, and thus also its temperature. The bridge voltage is the output of the device, in general consisting of a steady part V_{dc}, and a fluctuating component V_{ac}. The method is not suitable for field use because of the extreme fragility of the cylindrical sensors used so far (diameters of 25, 50, and 150 μm) and the adverse effect of deposits on the sensor from an unpurified medium. Moreover, random low-frequency flows in the surrounding medium influence the sensitivity in an unpredictable way, thus again limiting the use of the device to well-controlled laboratory conditions. An attempt was made to increase the ruggedness of the equipment by either of two methods, or a combination of both: on one hand, the use of sensors that are based on a more sturdy geometrical arrangement than the fragile quartz cylinders of small diameter; on the other hand, the packaging of the sensor in a rubber liquid-filled boot, as is common for the pressure-sensitive transducers developed and used at NRL-USRD.

In Refs. 1 and 2 it was mentioned that imposing a steady flow on the sensor by means of a nozzle improves the response of the sensor and holds the promise of a device that is independent of the direction of gravity, with the ability of detecting the direction of the particle motion by adjusting the orientation of the nozzle to maximum response. Further experiments have been performed to study the quantitative behavior of the effect for various values of the steady flow speed and temperature differences between sensor and medium.

The rugged sensor used in this study is shown schematically in Fig. 3. It is based on the deposition of a platinum film on a conical substrate and manufactured by Thermo Systems, Inc.

The drawings for the booted sensor and instruction for its assembly are given in the next section. This is followed by a description of the measurement and graphic presentation of the results.

The nozzle arrangement for imposing a bias flow is described, and the measurements for various flow speeds and temperature differences are discussed. The experiments in this study were done with the TSI Model IFA100 anemometer.

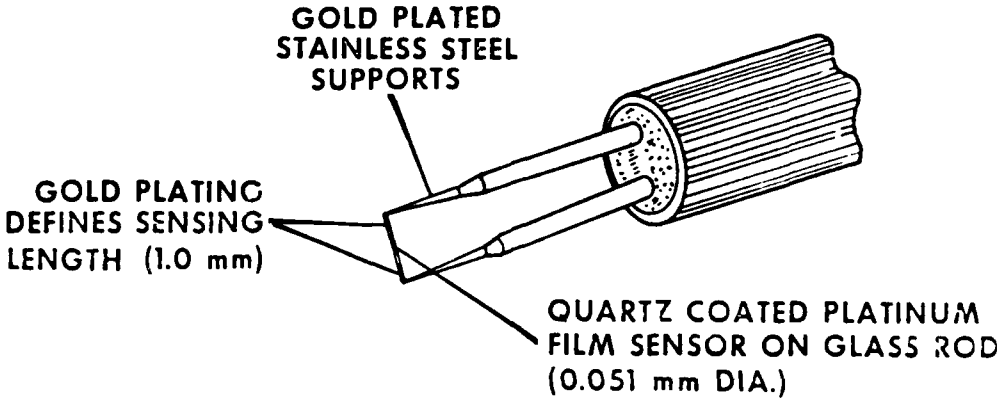

Fig. 1 - Cylindrical hot-film sensor.

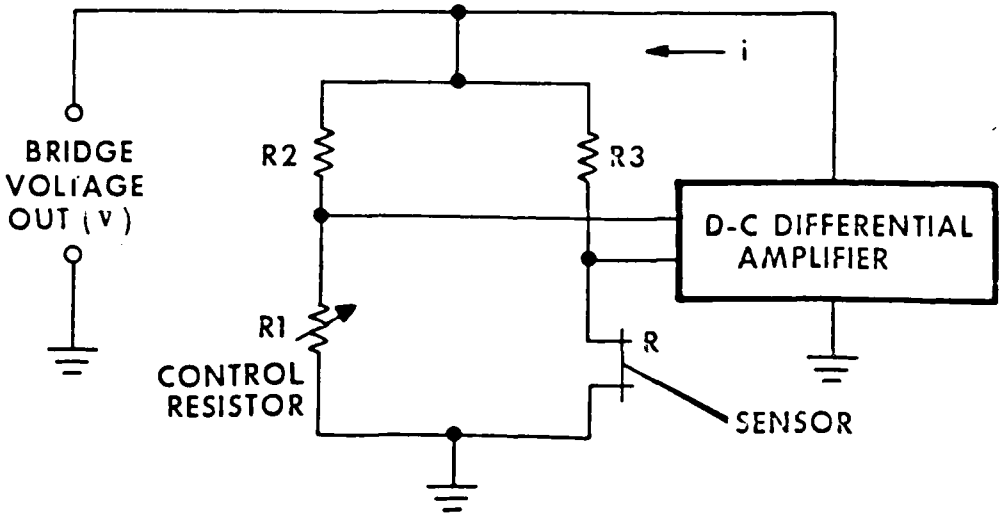

Fig. 2 - Schematic of constant temperature system.

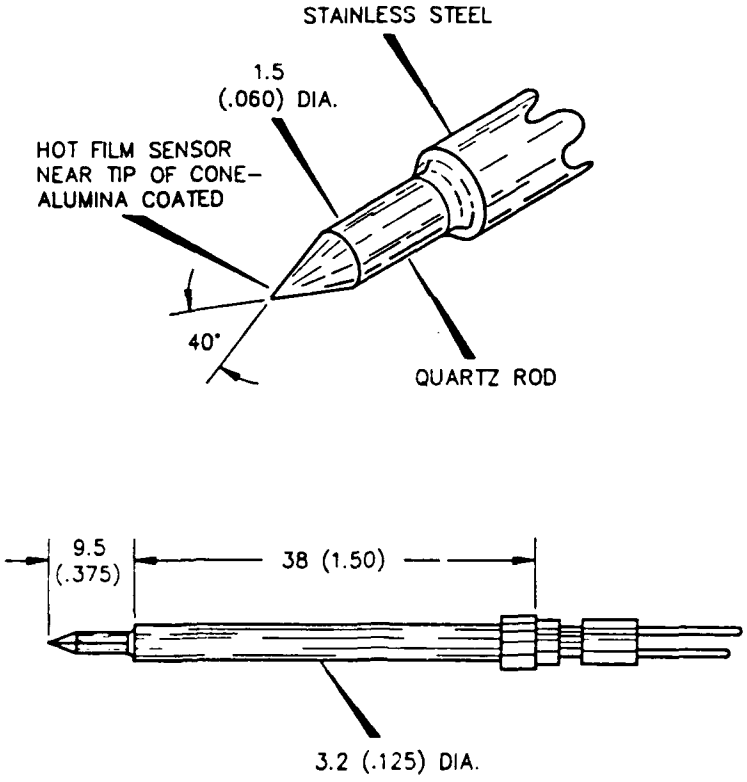

Fig. 3 - Detail sketch of a conical sensor, TSI Model 1230 [measurements in mm (inch)].

ENCLOSURE OF HOT-FILM SENSOR IN ELASTOMER BOOT

The hot-film sensor is enclosed in an elastomer boot to protect it from mechanical damage and fouling by the ambient acoustic medium. Figure 4 shows the main parts of this assembly. In Figure 5, the arrangement of the hot-film probe holder in the assembly is sketched. The boot assembly is shown in Fig. 6. Of course, the material of the boot may be varied. The effect of its elastic properties on the measurement is discussed in the next section. Figures 7 through 10 depict detailed parts of the assembly. Figures 11 and 12 show the spacer with the adapter and the insert. The sizes differ slightly depending on the use of a cylindrical or conical sensor, in order to match the location of the sensitive element to that of the ring on the outside of the boot (Fig. 6).

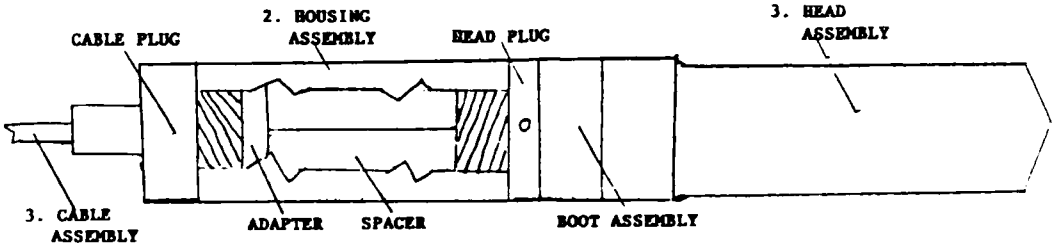

Fig. 4 - Booted hot-film anemometer.

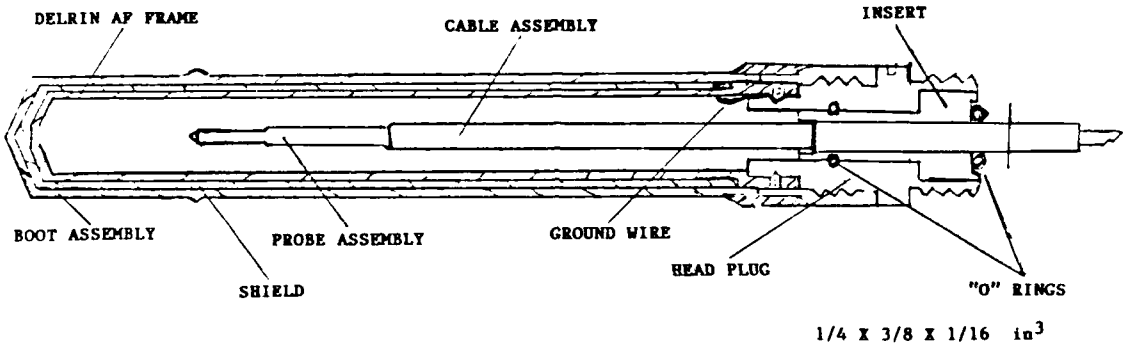

Fig. 5 - Head assembly.

Fig. 6 - Boot assembly.

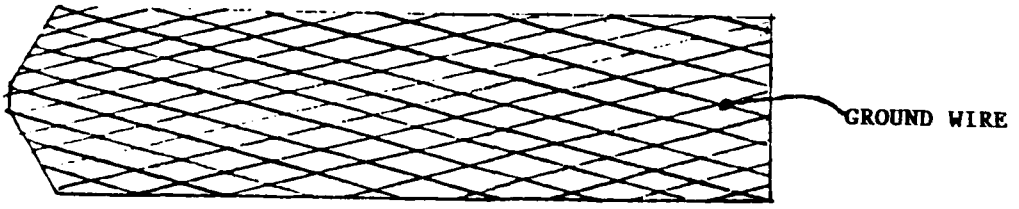

Fig. 7 - Shield.

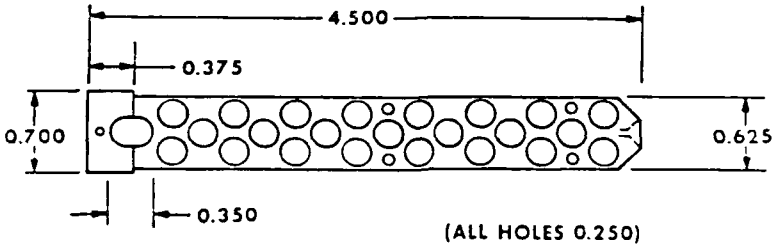

Fig. 8 - Delrin AF frame.

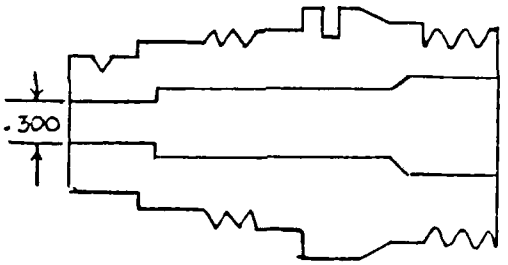

Fig. 9 - Head plug.

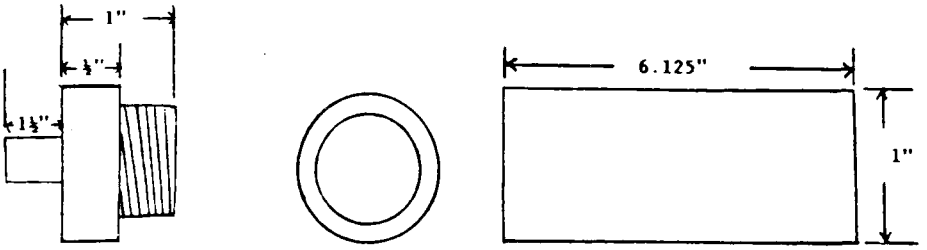

Fig. 10 - Cable plug.

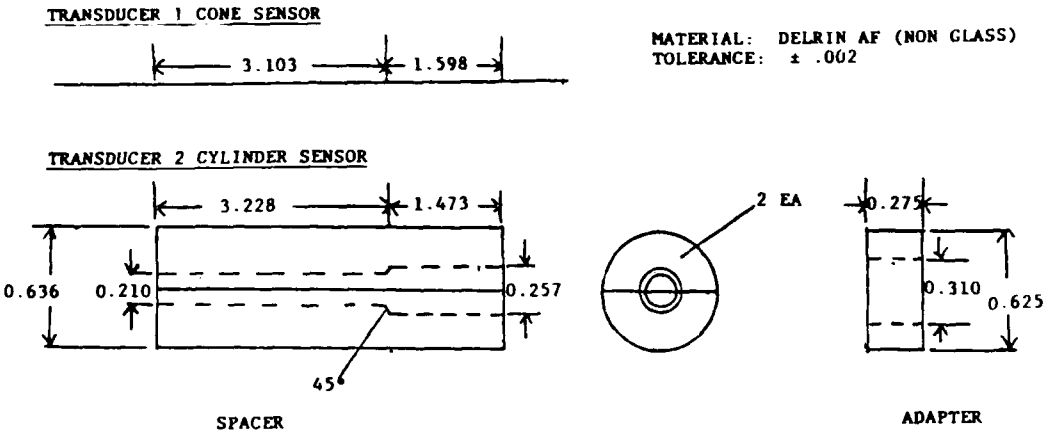

Fig. 11 - Spacer and adapter.

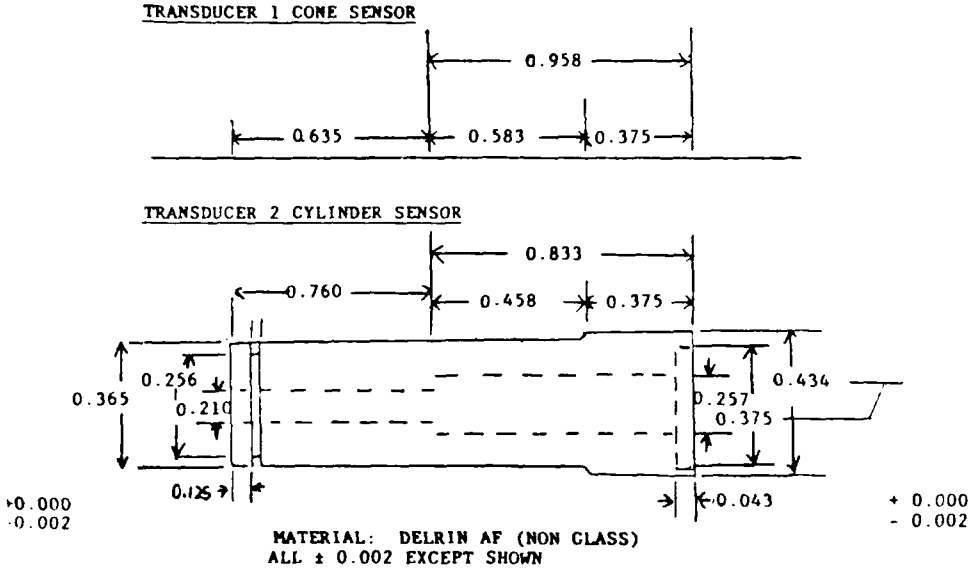

Fig. 12 - Insert.

INSTRUCTIONS FOR ASSEMBLING

Assembly of Cylinder Probe Transducer

- Degas a cup of deionized water in a vacuum of approximately 20 in. of mercury.
- Assemble the "Insert" (Fig. 3 and Fig. 10 - Transducer 2 cylinder sensor), to the "Head Plug" with the O-Ring installed.
- Feed the "Cable Plug" Housing, Adapter, and O-Ring over Cable Assembly in the order given.
- Guide the Cable through the "Insert."

- Plug in the "Probe Assembly" to the "Cable Assembly" making sure that the O-Ring is installed on the "Probe Assembly." Also be sure that the two male electrical pins are aligned with the "Cable Assembly" female electrical connector.

- Assemble a mu metal shield around the Delrin AF Frame, and solder a wire to the shield at the location where the wire will be mounted under one of the three Delrin AF Frame mounting screws.

- Guide the open end of the Delrin Frame over the "Probe Assembly," and mount the frame to the "Head Plug" with the three screws, making sure the tops of the screws are flush with the Delrin Frame.

- The wire from the shield must be mounted under one of the screws to ground the shield to the "Head Plug."

- Fill the "Boot Assembly" with the deionized water.

- Screw the "Boot Assembly" to the "Head Plug," being very careful not to let the "Cable Assembly" move out of the "Insert." Hold the "Boot Assembly" upright so that the water does not spill.

- Set the O-Ring in place at the end of the Head Plug.

- Assemble the "Spacers" (Fig. 2 and Fig. 9 - Transducer 2 cylinder sensor), around the cable and feed the "Housing" over the "Spacers" and screw into the "Head Plug." CAUTION: Do not spill the water!

- Assemble the Adapter, and screw the "Cable Plug" into the "Housing."

- Be very careful when assembling the transducer to keep the transducer full of water. Remove bubbles, and keep the cable assembly from pulling out of the "Head Assembly."

- This completes assembly of the transducer.

Assembly of Conical Probe Transducer

- Use assembly procedure above, with the difference in 2.B and 2.L below.

- Assemble the "Insert" (Fig. 3 and Fig. 10 - Transducer 1 conical sensor), to the "Head Plug" with the O-Ring installed.

- Assemble a mu metal shield around the Delrin AF Frame, and solder a wire to the shield at the location where the wire will be mounted under one of the three Delrin AF Frame mounting screws.

- Guide the open end of the Delrin Frame over the "Probe Assembly," and mount the frame to the "Head Plug" with the three screws making sure the tops of the screws are flush with the Delrin Frame.

- The wire from the shield must be mounted under one of the screws to ground the shield to the "Head Plug."

- Fill the "Boot Assembly" with the deionized water.

- Screw the "Boot Assembly" to the "Head Plug" being very careful not to let the "Cable Assembly" move out of the "Insert." Hold the "Boot Assembly" upright so that the water does not spill.
- Feed the "Cable Plug" Housing, Adapter, and O-Ring over the "Cable Assembly" in the order given.
- Plug the "Probe Assembly" into the "Cable Assembly" making sure that the O-Ring is installed on the "Probe Assembly." Also, be sure that the two male electrical pins are aligned with the "Cable Assembly" female electrical connector.
- Guide the Probe-mounted "Cable Assembly" through the "Insert."
- Set the O-Ring in place at the end of the "Head Plug."
- Assemble the "Spacers" (Fig. 2 and Fig. 9 - Transducer 1 conical sensor) around the cable and feed the "Housing" over the "Spacers" and screw into the "Head Plug." CAUTION: Do not spill the water!
- Assemble the Adapter, and screw the "Cable Plug" into the "Housing."
- Be very careful when assembling the transducer to keep the transducer full of water. Remove bubbles, and keep the cable assembly from pulling out of the "Head Assembly."
- This completes assembly of the transducer.

MEASUREMENTS AND DISCUSSION

The measurements were performed in the acoustic field created by a NRL-USRD type G40 calibrator, as described in detail in Refs. 1 and 2. The pressure field in the calibrator is determined by an F61 standard pressure hydrophone. At the present accuracy of the measurement it is sufficient to measure the pressure at a given depth and to evaluate the velocity profile by means of the added knowledge that the pressure is zero at the liquid surface of the calibrator. To reduce the effect of long-term drift in the measurements, the HFA and pressure hydrophone were both inserted into the calibrator, and measurements from both detectors were taken by turns under computer control.

The bridge voltage V_{ac} of the HFA is found as a function of frequency. The pressure measurement provides a measure of velocity or displacement of the fluid particles. Previous experience indicated that for vertical particle motion the output voltage is proportional to the (vertical) displacement ζ, and thus the data are represented by

$$V_{ac} = a_V \, (\zeta/d) \, , \qquad (1)$$

where d is the diameter of the hot-film sensor. The factor a_V is independent of the frequency for a wide range of experimental parameters, at least for a cylindrical, bare sensor. This is shown in Fig. 13 for a model 1210-20W

sensor, with a temperature difference between sensor and medium of 30°C. Figure 13a gives the magnitude of a_V and Fig. 13b the phase relative to the phase of the pressure measurement. The dots in Fig. 13a are for the bare sensor; the dashed line is the average of the individual points. Although the data are noisy, one sees that the assumption of constant a_V is reasonably well satisfied. The solid curves are those for the booted sensor. The fill fluid is water. They show a pronounced resonance near 135 Hz, which is tentatively ascribed to axial vibrations of the rubber boot with fill fluid. At higher frequencies the curve appears to merge with the constant a_V value for the bare sensor. It is possible that this resonance feature is connected with the shift in effective center of several NRL-USRD hydrophones, dependent on frequency, that was observed before.

The voltage response goes to zero for zero frequency, since the boot will not transmit a steady flow. Identification of the resonance with vibrations of the boot is supported by the results after replacing the butyl rubber boot by one made of a more compliant gum rubber; the resonance peak shifts from 135 Hz down to 45 Hz.

The figures show, moreover, that there is much less noise in the data of the booted sensor as compared with the bare sensor. This is probably due to the reduction of the effect of low-frequency spurious flows in the medium by the boot.

In the given experiment the fill fluid was water, the same as the acoustical medium. The water in the boot was deionized and degassed, which avoided problems with deposits of contaminations on the sensor and also prevented the formation of air bubbles on the sensor, which are very troublesome with a bare sensor in a medium open to air. One might consider using other fill fluids chosen with an eye on improving the sensitivity of the sensor. Any possible advantage in this respect is probably offset by the ensuing mismatch in acoustical impedance between medium and fill fluid.

An alternate way to improve the ruggedness of hot-film sensors is to employ a sensitive element (platinum film) deposited on an extended substrate of conical, wedge, or hemispherical shape. Figure 1 shows the geometry of a conical sensor.

Measurements were performed with this sensor in the G40 calibrator. The displacement of the fluid particles ζ is taken relative to d, where d is the diameter of the ring-shaped platinum film on the cone. It has the value 300 μm, or six times the value of the sensor diameter of the cylindrical sensor used before.

Figure 14 shows the results for the coefficient a_V as a function of frequency. The most striking result here is that the a_V increases with frequency in contrast to the case of the cylindrical sensor. The dependence is roughly proportional to frequency, which would imply that not the displacement but the velocity is the parameter to which the voltage output is proportional. Apparently the flow regime about the sensor is different in the present case: one might think of the different geometry as the cause, but it is more probable that the reason has to be sought in the greatly increased Rayleigh number. With the cylindrical sensor it was discovered that the dependence of "a,"

defined as the ratio of ac Nusselt number to relative displacement, was a function of the Rayleigh number. The Rayleigh number is proportional to the third power of the characteristic length; the ratio of these lengths between cylindrical and conical sensors is six. Thus the regime for the cylindrical sensor, where Ra was smaller, or at most equal to one, (Ra = 0.14 for the case of Fig. 13) is now replaced by a much larger value (Ra = 30 for Fig. 14) indicating that viscosity domination in the first case has been replaced by inertia domination, or possibly boundary-type flow, in the second case. An alternative or additional factor to explain the dependence on velocity is found in the second part of this report.

Thus the conical sensor misses one advantage of the thin cylindrical one. The latter increases in sensitivity, for fixed acoustic intensity, when lowering the frequency. This is in favorable contrast with most pressure transducers in which the sensitivity drops off at lower frequency.

The conical sensor by itself is much more rugged than the cylindrical ones. Packaging the conical sensor would, of course, add the advantages of this technique. The voltage output, not normalized by reference to sensor diameter, though, is considerably less than that of the cylindrical sensor.

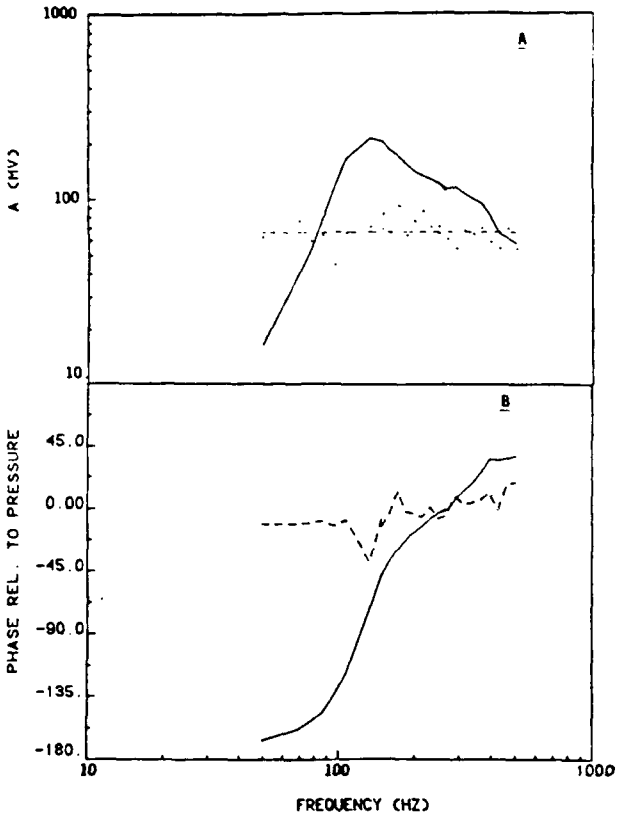

Fig. 13 - Coefficient a_v in relation of HFA output to relative particle displacement, for a cylindrical sensor. a - magnitude; b - phase; - - - - - bare sensor; _____ booted sensor. Difference in temperature between sensor and medium is 30°C.

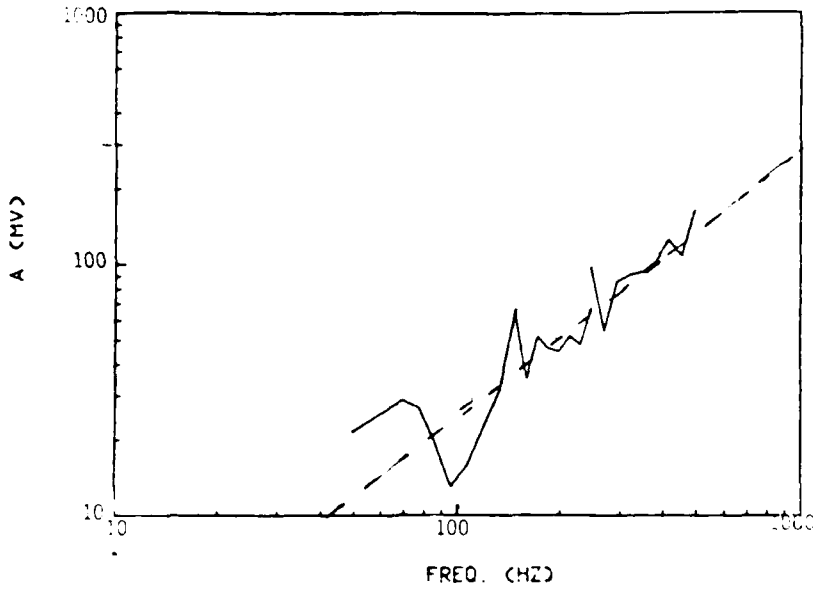

Fig. 14 - Magnitude of coefficient a_V in relation of HFA output to relative particle displacement, for a conical sensor. - - - - - trend line proportional to frequency. Temperature of sensor is 30°C above ambient.

IMPOSED BIAS FLOW

If there is no acoustic field the hot film will be cooled by conduction and convection, and a constant dc voltage is measured on the bridge. The convection in this case is so-called free convection, caused by the rising of the heated and, therefore, lighter liquid in the earth's gravitational field. This vertical convection functions as a vertical dc bias flow, that increases the sensitivity for particle motion in the vertical direction. (It also causes the output frequency to be equal to the frequency of the acoustic field, in contrast to the case of horizontal particle motion.)

This role of free convection in the forming of the output signal led to the notion that the creation of an imposed flow directed onto the sensor might possibly improve the response of the device to acoustic particle motion, in the direction of the flow. This would lessen the dependence on the direction of gravity and, moreover, would enable one to find the direction of the acoustic wave motion by changing the orientation of the imposed flow until a maximum response is obtained.

The imposed flow was realized as a free jet issuing from a nozzle. The flow is gravity driven by means of a container at a higher level to ensure a smooth laminar flow. It may be regulated by a needle valve.

The sensor and nozzle arrangement is shown in Fig. 15. A semicircular arch (1) is rigidly connected to a circular rod (2). A second semicircular arch (3) is hinged with respect to the arch (1) such that it can rotate about the axis A--A. This movable arch (3) supports a nozzle (4). A flexible hose (5) is attached to the nozzle and supplies liquid under pressure, which issues

from the nozzle opening (6) as a well defined jet. The jet flow from the nozzle opening (6) impinges on the hot-film sensor (7) aligned along the axis A--A. The sensor (7) is held by a probe holder (8) which is directly attached to a coaxial cable (9). This coaxial cable (9) provides the link between the sensor and the electronic instrumentation.

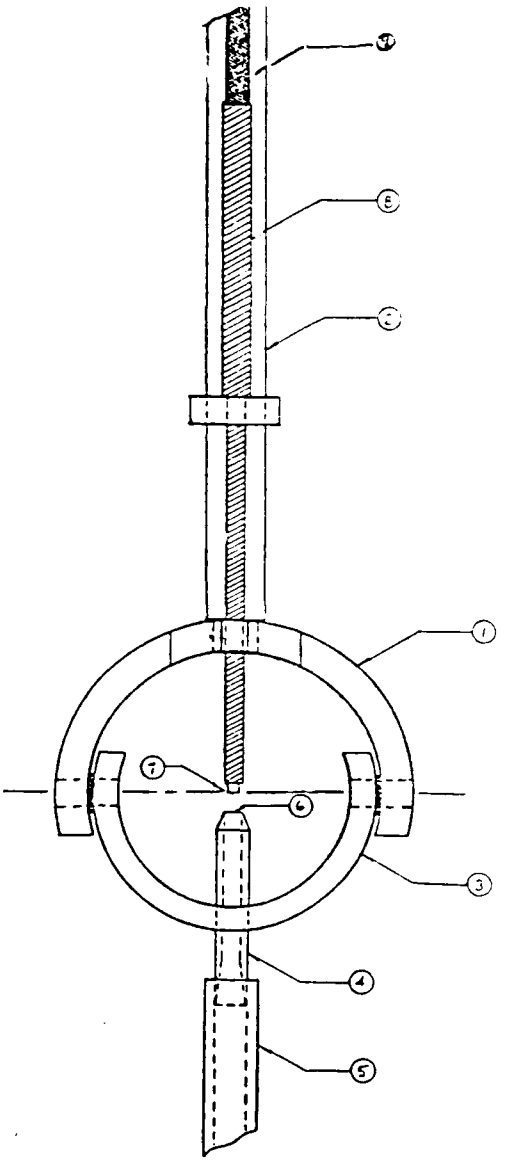

Fig. 15 - Front view of nozzle arrangement for imposed bias flow.

VELOCITY CALIBRATION

The HFA was calibrated for steady flow by means of a water-filled circular tank placed on a rotating disk driven at its edge by a friction-coupled, variable speed, drill motor. The velocity v at distance r from the center of the tank is simply computed by $v = \omega r$, after sufficient time has elapsed to establish solid body rotation for the liquid. Here ω is the angular frequency of rotation.

Figure 16 shows the results of the calibration of a TSI 1212-60W sensor (S/N #L598). The squares are the experimental points for a temperature difference $\Delta T = 30°C$ between sensor and medium, the circles for $\Delta T = 45°C$. Without an imposed bias flow there still is the free convection flow, the speed of which may be estimated by dimensional analysis, as described in Ref. 1. One finds for v connected with free convection a value of 0.39 cm/s at $\Delta T = 30°C$, and of 0.54 cm/s for $\Delta T = 45°C$. These points are also shown in Fig. 16. One should keep in mind, though, that the character of the flow field is different for the two cases of free convection and imposed flow. For the latter the speed of the flow approaches the nominal speed of the jet at large distances from the sensor, compared with the sensor diameter; while in the former the speed approaches zero away from the sensor.

The solid curves in the figure are a fit to the experimental data of the form $V_{dc}^2 = a + b\, v^{0.5}$ (King's law), where V_{dc} is the steady bridge voltage (in volts) as a response to a steady flow with speed v (cm/s). The coefficients a and b were determined by least squares. Only the points 2 through 6 of each nine-point set were used in the adjustment. One finds $a = 4.78$ and $b = 5.59$ for $\Delta T = 30°C$, while $a = 6.45$ and $b = 8.67$ for $\Delta T = 45°$.

One may compute the speed of the free convection flow by setting V_{dc} equal to its value for the no-imposed-flow condition, and solving for v. Thus one finds a speed of 0.16 cm/s for $\Delta T = 30°C$ and 0.44 cm/s for $\Delta T = 45°C$. The latter value concurs well with the estimate given above, the former less so.

By means of this calibration one can establish the speed of the impacting jet of liquid by observing the value of the output dc voltage of the anemometer. The five points for which experiments were performed are shown as pluses on the two curves of Fig. 16.

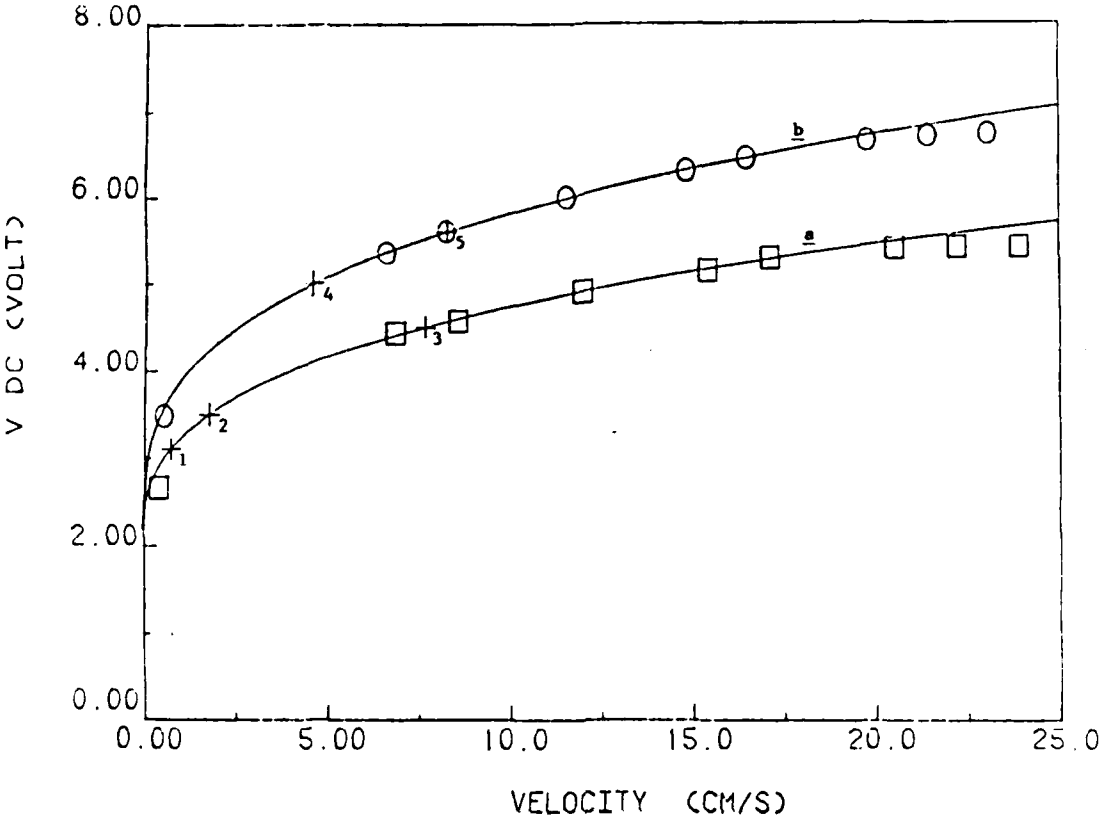

Fig. 16 - Velocity calibration of TSI 1212-60W sensor (serial #L598). Sensor diameter = 150 μm.

□□□ $\Delta T = 30°C$ solid curve a: $V_{dc}^2 = 4.78 + 5.59 \sqrt{v}$

000 $\Delta T = 45°C$ solid curve b: $V_{dc}^2 = 6.45 + 8.67 \sqrt{v}$

+++++ Operating points for experiments, 1 through 5 corresponding to the results shown in Fig. 17 curves 1, 2, and 3, and Fig. 18 curves 1 and 2, respectively.

RESPONSE TO HYDROACOUSTIC FIELD

The response of the HFA to a hydroacoustic field, under imposed bias flow was tested in a G40 calibrator, as was the case for the experiments described earlier in this report. The velocity field in the calibrator was determined by a USRD type F61 standard hydrophone, according to Euler's equation $\partial w/\partial t = -(1/\rho)\partial p/\partial z$, where p is the pressure at depth z, ρ the density of the liquid in the calibrator, and w the vertical particle velocity. It is assumed that $kz \ll 1$, where k is the wavenumber in the liquid.

The results of the calibration were not quite satisfactory and in poor correspondence with the results of earlier calibrations. It was judged that the ratios of anemometer output with the jet flow turned on over those without flow would be more reliable than output values normalized by the calibration result. Therefore, these ratios are shown in the following figures. The discrepancy of new and old calibration data in the anemometer data without flow might be due to diffraction about the nozzle arrangement; this point should be more carefully studied.

A comparison was made between the ac voltage output when the nozzle is directed 90° to the vertical with and without flow. The results are rather noisy, but one appears entitled to conclude that the ratio does not essentially differ from zero. A residual effect of the flow may exist, of course, since the jet could "blow" the thermal convective plume to one side and thus influence the response of the sensor to vertical particle motion.

Measurements were performed with the nozzle pointing straight up for $\Delta T = 30$ and 45°C. The results for $\Delta T = 30$°C are shown in Fig. 17. In addition to the no-flow condition, the anemometer dc voltages were set at 3.1, 3.5, and 4.5 V, which correspond to 0.75, 1.79, and 7.7 cm/s flow speed by the calibration curves of Fig. 16. Similarly, Fig. 18 shows the results for $\Delta T = 45$°C with voltage settings of 5.0 and 5.6 V, corresponding to flow speeds 4.6 and 8.3 cm/s. These operating points are also shown in the calibration curves of Fig. 16.

Former experience with hot-film ac response [1, and 2] indicated that for most of the measurements, for a large range of experimental parameters, the anemometer output was proportional to the displacement of the fluid particles. One sees in Fig. 17, curves 1 and 2, that the ratio is practically independent of frequency, and thus the same proportionality to displacement appears to apply to imposed flow speeds of 0.75 and 1.79 cm/s. It may be pointed out that these flow speeds are close to the free convection flow speed, which, in Ref. 1 (Table I, p. 8), was estimated as 0.39 cm/s. For the higher flow speed, 7.7 cm/s of curve 3 in Fig. 17, the trend is clearly to a positive slope. This behavior persists in Fig. 18, for $\Delta T \approx 45$°C, where curve 2 for a flow speed of 8.3 cm/s comes close to a slope of 1, which would indicate proportionality of the output to the particle speed rather than to displacement. For comparison, the free convection flow speed in this case was estimated in Ref. 1 to be 0.54 cm/s.

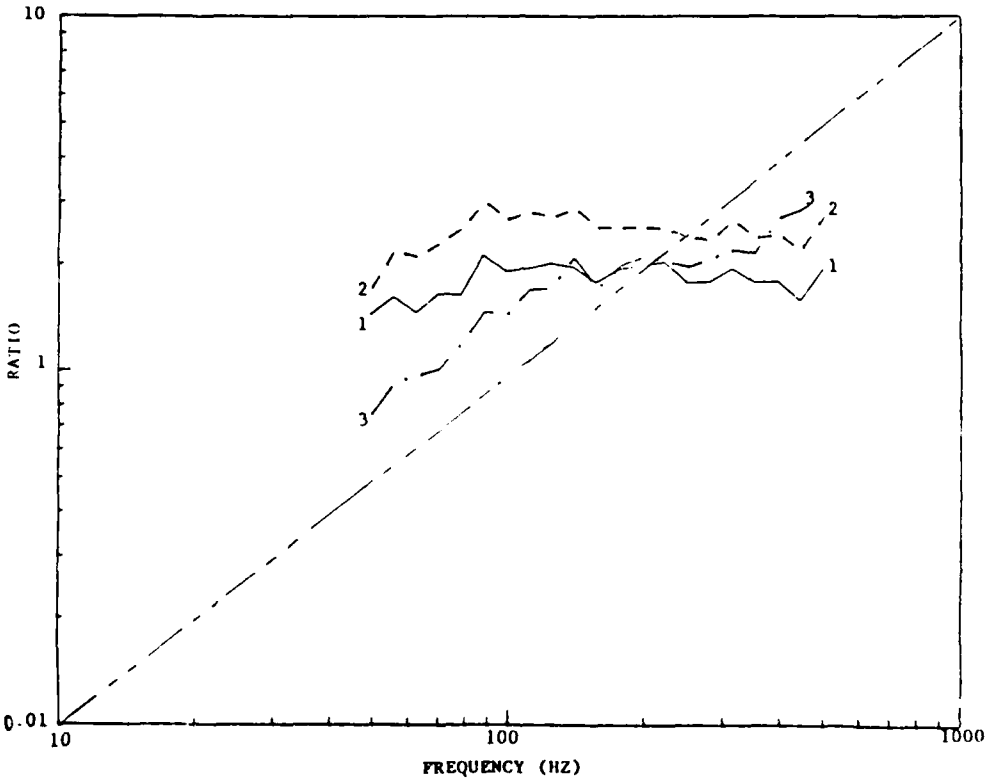

Fig. 17 - Ratio of anemometer ac voltage under imposed flow to output without flow. $\Delta T = 30°C$.

1. $V_{dc} = 3.1$ V; v = 0.75 cm/s
2. $V_{dc} = 3.5$ V; v = 1.79 cm/s
3. $V_{dc} = 4.5$ V; v = 7.7 cm/s

-----trend line proportional to frequency

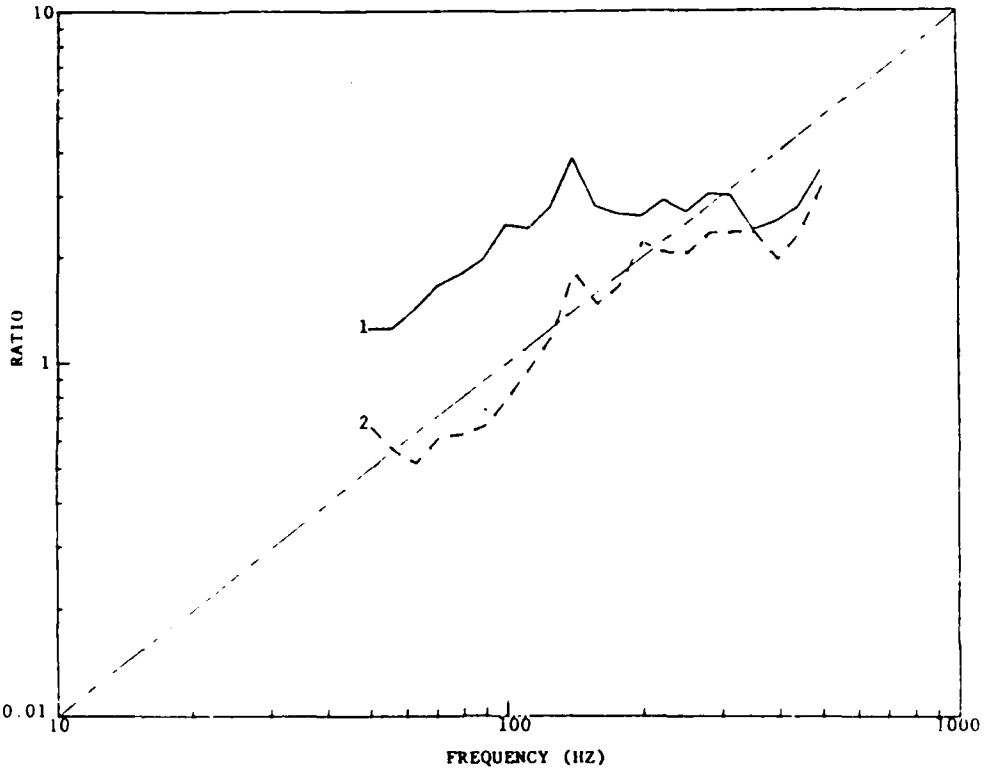

Fig. 18 - Ratio of anemometer ac voltage output under imposed flow to output without flow. $\Delta T = 45°C$.

1. $V_{dc} = 5.0$ V; v = 4.6 cm/s
2. $V_{dc} = 5.6$ V; v = 8.3 cm/s

-----trend line proportional to frequency

DISCUSSION OF RESULTS

Hot-film or hot-wire anemometry is often used in determining turbulence spectra in gases and liquids. It is common to calibrate the device by measuring the voltage response as a function of dc flow, as was done in this study (shown in Fig. 16). This dc curve is then applied to the interpretation of turbulence spectra without a discussion of possible dynamic effects on the heat transfer process by the fluctuating flow (see for example Ref. 3). Manufacturers of HFA equipment even supply an electronic linearizer with adjustable polynomial coefficients that imitates the dc calibration curve.

The experiments discussed here indicate that this procedure may be limited to certain ranges of the relevant parameters. One would imagine that for low frequency the ac response tends to the dc response, so that use of the dc calibration curve would be allowed. For increasing frequency, though, one would expect deviations from this calibration. One could justify this expectation by referring to the concept that fluid particles subject to a fluctuating velocity component will repeatedly pass by the hot wire or film, which results in a particle temperature that is essentially higher than the

ambient medium, thus reducing the heat transfer. In this picture, a larger displacement would constitute better cooling. A measure for the size of this effect can be obtained by comparing the order of magnitude of the local heating, proportional to $\partial T/\partial t$ with the estimate of convective cooling by the dc flow, proportional to $v\ \partial T/\partial z$. This leads to a dimensionless number $\omega d/v$ that is deemed responsible for the behavior of the anemometer under various circumstances of frequency ω, imposed dc flow speed v, and sensor diameter d.

It is expected that a transition between the two regimes (proportionality to speed or displacement of the fluid particle) would take place at a value of the frequency such that this dimensionless number $\omega d/v$ is of order one. For Fig. 17 (curves 1, 2, and 3) these critical values for f_c are 8, 19, and 81 Hz, respectively, which would explain why curves 1 and 2 have proportionality to displacement, while curve 3 shows a tilt toward proportionality to speed. In Fig. 18 the values for f_c (corresponding to curves 2 and 3) are 48 and 86 Hz, respectively. With some imagination one might claim that both figures show a transition from a slope of zero to a slope of one at values in the range of these frequencies.

It was attempted to merge the curves of Figs. 17 and 18 into a single curve by the following considerations. The transition of the ratio of voltages from proportionality to ω to independence from ω suggests a relaxation type factor $i\omega\tau/(1 + i\omega\tau)$, where τ is a relaxation time of order d/v. The absolute value of this factor is

$$\frac{\omega\tau}{\sqrt{1 + \omega^2\tau^2}} \quad . \tag{2}$$

For free convection flow in the frequency range of the measurements this factor is close to one. Therefore, one expects an adjustment of the various curves in the abscissa by plotting the results as a function of a dimensionless frequency $\Omega = \omega d/v_i$, where v_i is the imposed flow speed.

The scaling for the ordinate is found by reference to the relationship between the ac Nusselt number Nu_{ac} and the vertical particle displacement ζ, which is expressed by [1, 2]

$$Nu_{ac} = a\ (\zeta/d) \quad . \tag{3}$$

The coefficient a was found to be given by $a = 0.21\ Ra^{0.42}$, where Ra is the Rayleigh number. The ac Nusselt number is given by $Nu_{ac} = 2\ Nu_{dc}\ V_{ac}/\ V_{dc}$, and, in turn, Nu_{dc} is proportional to V_{dc}^2. Other factors in Nu_{dc} cancel out in the ratio of voltages.

The Rayleigh number in the context of free convection appears as a modified Péclet number, $Pe = vd/\kappa$, where κ is the thermal diffusivity; it represents the ratio of heat transfer by convection to that by conduction. For free convection the flow speed is not a priori given and has to be estimated by balancing the viscosity term and the buoyancy term in the equation of motion (for viscosity-dominated convection). This results in the Rayleigh number as

the expression for the ratio of heat transfer by convection to that by conduction. To adapt this heat transfer ratio to the mixed case of free convection and imposed bias flow, it is suggested to replace the Rayleigh number by Ra (v_i/v_f), where v_f is the free convection flow speed, and thus to set $a = 0.21\ Ra^{0.42}\ (v_i/v_f)^{0.42}$. In summing up, if one takes the ratio of Eq. (3) for imposed flow and free convection, one expects a functional relationship

$$\frac{(V_{ac})_i}{(V_{ac})_f}\ \frac{(V_{dc})_i}{(V_{dc})_f} = \left(\frac{v_i}{v_f}\right)^{0.42}\ \frac{s\Omega}{\sqrt{1 + s\Omega)^2}}\ , \tag{4}$$

where s is an adjustable constant of order one in the relation $\tau = sd/v$.

This suggests that merging of the curves of Figs. 17 and 18 may be accomplished by multiplying the ratio of voltages for imposed bias flow to free convection by $(V_{dci}/V_{dcf})\ (v_f/v_i)^{0.42}$ and plotting the results as a function of $\Omega = \omega d/v$. This is shown in Fig. 19. The values for v_f used in the ratio reduction were computed according to King's law, as described before (0.16 cm/s for $\Delta T = 30°$, and 0.44 for $\Delta T = 45°$). This results in a better overall fit of the data than if one takes the values for v_f from dimensional analysis. By visual inspection a curve

$$\frac{s\Omega}{\sqrt{1 + s^2\Omega^2}}\ , \tag{5}$$

with factor s = 0.5 was fitted to the data, also shown in Fig. 19. One sees that there is considerable noise in the data, but the suggested general frequency dependence seems to be present. The factor $\frac{1}{2}$ for s implies that the characteristic time constant is given by $\tau = \frac{1}{2}\ \omega d/v = \omega R/v$ where R is the radius of the sensor.

The relaxation type of behavior would also indicate a phase shift of 90° in the ratios when going from low to high frequency. Phase was not consistently measured, but some casual observations appear to confirm this. It is not clear at this time whether the dependence of voltage output to particle velocity found for a conical sensor (discussed earlier) is related to the effect described above. The size of the conical sensor leads to inertia-dominated flow, with a concomitant boundary layer; and this regime has to be studied on its own merits.

The implication of the dynamic behavior of the anemometer for interpretation of turbulence measurements may be illustrated by a simple example. Suppose one wants to measure turbulence spectra in pipe flow at a Reynolds number of 10,000, above the critical Re for turbulence. With water in

a 1-cm diam. pipe, one finds a flow speed of 100 cm/s. Given a sensor diameter of 50 μm (three times smaller than the one used in this study), the critical frequency $f_c \simeq 3$ kHz. For air, the kinematic viscosity is on the order 10 smaller. Thus with a hot wire of the same diameter, one finds $f_c \simeq 30$ kHz (admittedly, one can use thinner wires in gases). In view of the fact that it is claimed that the constant temperature anemometer can give valid response up to 300 kHz, it follows that for some individual cases one has to decide whether possibly part of the measured spectra might be influenced by the dynamic effect of a velocity response that is a function of frequency. For the usual situation in air, the critical frequency will be very high, and thus the dc calibration is acceptable.

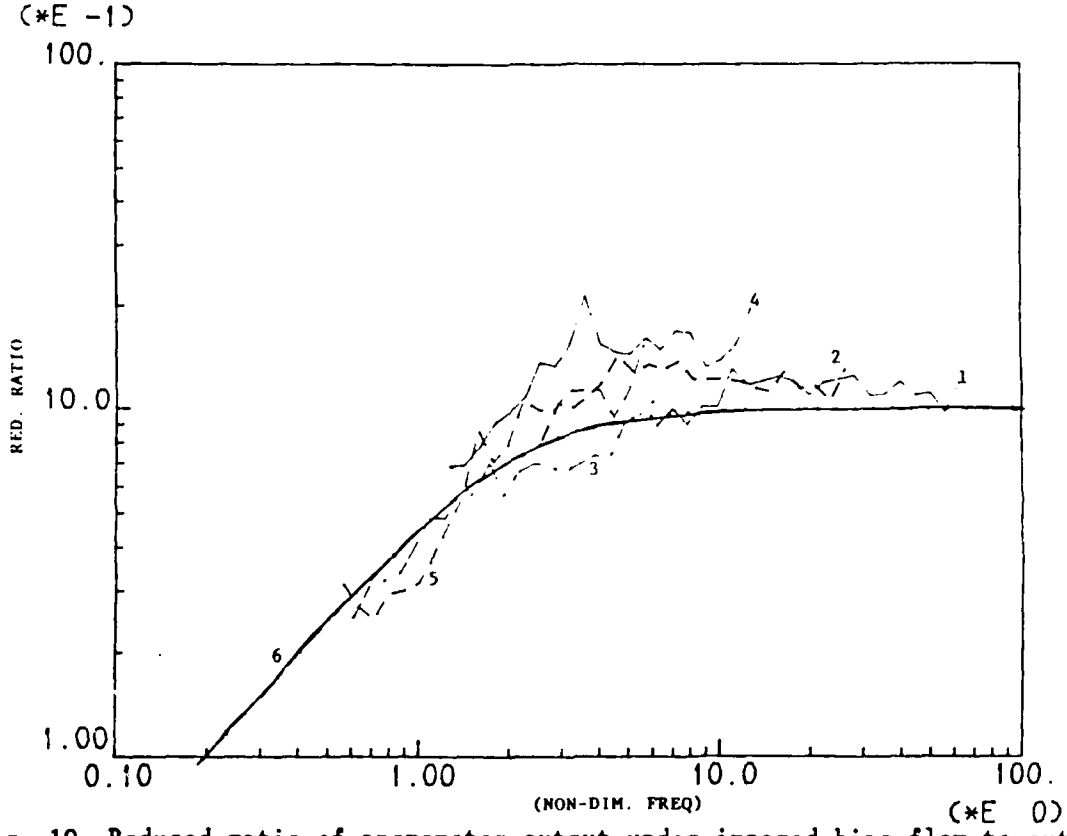

Fig. 19. Reduced ratio of anemometer output under imposed bias flow to output without imposed flow, as a function of dimensionless frequency, $\Omega = \omega d/v$.

1. $\Delta T = 30°$, v = 0.75 cm/s
2. $\Delta T = 30°$, v = 1.79 cm/s
3. $\Delta T = 30°$, v = 7.7 cm/s
4. $\Delta T = 45°$, v = 4.6 cm/s
5. $\Delta T = 45°$, v = 8.3 cm/s

6. adjusted curve $0.5\Omega/\sqrt{1+0.25\Omega^2}$

CONCLUSIONS AND RECOMMENDATIONS

The results from the booted sensor indicate that one can make the HFA into a device that can be used for particle motion in hydroacoustic fields outside the strictly controlled conditions of a laboratory.

The experiments with imposed bias flow show that the voltage output proportional to particle displacement, typical for the case without imposed flow, can be amplified by an imposed flow up to a certain amplification factor which, in this set of experiments, was not higher than about three.

For sufficiently low-frequency or high imposed flow speed the dependence of the voltage output tends to be proportional to particle speed rather than particle displacement. This transition is governed by the dimensionless number $\omega d/v$; where ω is the angular frequency, d the diameter of the sensor, and v the imposed velocity. The transition occurs where this number is of order one.

It would be desirable to extend the experiments with better accuracy, especially with sensors of different diameters. In general, it would be worthwhile in the picture to study the origin of the noise in the data, and to possibly reduce the signal-to-noise ratio.

The dynamic effect of a fluctuating flow on the anemometer response necessitates consideration of the correctness of using the dc HFA calibration curve for ac applications.

REFERENCES

1. P. S. Dubbelday, "Measurement of Hydroacoustic Particle Motion by Hot-Film Anemometry," NRL Memorandum Report 5223, Feb 1984.

2. P. S. Dubbelday, "Hot-film anemometry measurement of hydroacoustic particle motion," J. Acoust. Soc. Am. 79, 2060-2066, (1986).

3. P. Bradshaw, "An Introduction to Turbulence and Its Measurement," (Pergamon, Oxford, 1971) pp. 116-117.